Thermal Preconditioning and Restoration of Bismuth-Containing, Lead-Free Solder Alloys

ANDRÉ M. DELHAISE [1,7] POLINA SNUGOVSKY,[1] JEFF KENNEDY,[1]
DAVID HILLMAN,[2] IVAN MATIJEVIC,[3] STEPHAN MESCHTER,[4]
DAVID ADAMS,[2] MILEA KAMMER,[5] MARIANNE ROMANSKY,[1]
JOSEPH JUAREZ,[5] IVAN STRAZNICKY,[6] LEONID SNUGOVSKY,[3]
ROSS WILCOXON,[2] and DOUG D. PEROVIC[3]

1.—Celestica, Inc., Newmarket, Canada. 2.—Collins Aerospace, Cedar Rapids, USA.
3.—Department of Materials Science and Engineering, University of Toronto, Toronto, Canada.
4.—BAE Systems, Farnborough, UK. 5.—Honeywell Aerospace, Phoenix, USA. 6.—Curtiss-
Wright, Davidson, USA. 7.—e-mail: dr.andre.m.delhaise@gmail.com

Bismuth (Bi)-containing solder alloys have emerged as prime candidates to replace traditional lead (Pb)-free alloys such as SAC 305 (Sn-3.0Ag-0.5Cu, in wt.%); unlike SAC alloys, these alloys show stability in mechanical properties after aging. A process was developed in which a Bi-bearing alloy is intentionally subjected to a short above-solvus thermal treatment, to potentially extend the life of the solder joint and improve device reliability. This treatment may be implemented after reflow, or periodically in service as a form of preventive maintenance. In this work, we evaluated this treatment as both a preconditioning and restoration process to compare Violet (Sn-2.25Ag-0.5Cu-6.0Bi, in wt.%) and SAC 305 alloys. Firstly, the solvus temperature of Violet was evaluated experimentally; this result was used to determine an appropriate heat treatment temperature for preconditioning and restoration. It was found that the heat treatment produces a highly equiaxed β-Sn grain structure, likely caused by particle stimulated nucleation during Bi precipitation. The creep resistance of the alloy was found to improve after the treatment. Finally, it was observed that both Bi and preconditioning can have varying effects on the thermal cycling reliability of the alloy, depending on the harshness of the thermal cycle (ΔT).

Key words: Bismuth, preconditioning, restoration, thermal cycling, creep

INTRODUCTION

There has been significant interest in the development, characterization, and testing of lead (Pb)-free solder alloys since the inception of the Restriction of Hazardous Substances Directive (RoHS). More recently, third-generation solder alloys have emerged due to the many shortcomings of traditional materials consisting primarily of tin (Sn), with small additions of silver (Ag) and copper (Cu). These include increased manufacturing costs and carbon footprint due to the higher melting point over Sn-Pb, increased damage to printed circuit board (PCB) and components due to high-temperature excursions during assembly, poor reliability in harsh environments, and susceptibility to Sn whiskers, as well as degradation of microstructure and mechanical properties during service life (aging) of components.[1,2] Several alloying elements have been identified in third-generation alloy development efforts to address these issues, including antimony (Sb), indium (In), and bismuth (Bi).[3]

Bi is a particularly attractive alloying element for Pb-free alloys, for several reasons. Additions of even small amounts of Bi suppress the melting point of Sn and SAC alloys,[4] reducing energy consumption and thermal damage during assembly. Bi has shown to improve wetting characteristics in both Sn-Ag[4] and SAC alloys,[5] and the addition of Bi to Sn-Ag and SAC alloys has also been shown to improve mechanical properties such as tensile[6] and shear[4] strength. Bi-bearing alloys also tend to perform better in harsh reliability testing compared with SAC alloys,[7] and preliminary research has suggested that Bi may mitigate against tin whisker formation.[8] Finally, Bi forms a simple binary eutectic system with Sn, with no brittle intermetallic compounds (IMCs), and can induce solid solution strengthening at low Bi content, and precipitation at high Bi content.

These alloys are also substantially more robust than SAC after aging. Witkin performed tensile testing on two Bi-containing alloys (Sn-3.4Ag-4.8Bi and Sn-3.3Ag-1.0Cu-3.4Bi; in wt.%) at several temperatures and found that both yield and ultimate tensile strength underwent little change after aging at 150°C for 336 h.[6] The tensile properties of SAC 305, on the other hand, were strongly affected by aging. In a separate study, Witkin observed similar trends with the same alloys with respect to creep strain rate and aging.[9] Examination of alloy microstructure revealed that this "stabilization" effect on the properties of the alloy after aging is accompanied by a very uniform dispersion of Bi precipitates,[10,11] suggesting that, during aging, Bi enters into solid solution with β-Sn and migrates from the interdendritic spaces into precipitate-free dendrites via solid-state diffusion.

It is evident from examining aging studies in the literature that Bi is a highly mobile species, even at room temperature. This may be of some concern owing to the highly anisotropic nature of the β-Sn body-centered tetragonal lattice, as well as the tendency for Pb-free solder joints to nucleate in random orientations after reflow.[12] Recent work examining solid-state diffusion has shown that the diffusivity of Bi in β-Sn is not highly anisotropic,[13,14] which is a welcome finding with respect to long-term reliability.

TEST OVERVIEW AND OBJECTIVES OF STUDY

It is evident based on prior experiments with isothermal aging that Bi-containing alloys may be more robust and durable in service. However, it was also observed that the initial microstructure of Bi-containing alloys may be relatively nonuniform. In addition, during lower temperature aging, such as at room temperature, Bi precipitates may undergo coarsening[11]; these larger precipitates are likely less effective second phase strengtheners in the alloy than a fine dispersion,[15] which is observed after high-temperature aging.

Elevated temperature aging, which has been consistently demonstrated to degrade the mechanical properties and reliability of SAC and SnPb, appears to improve the microstructure and stabilize the mechanical properties of Bi-containing alloys. It was hypothesized, therefore, that by deliberately subjecting Bi-containing solder joints to a high-temperature heat treatment, a more homogenous microstructure could be formed, which may prolong the life of the alloy. Such a heat treatment could, in theory, be strategically implemented at various points in the life cycle of the alloy, when the microstructure becomes less desirable. For example, after assembly, a preconditioning heat treatment could drive the interdendritic Bi into the β-Sn dendrites, and after some time in service, a restorative heat treatment might dissolve coarse Bi precipitates and induce reprecipitation of finer precipitates.

The goal of these studies is to characterize the heat treatment as a preconditioning and restorative process. Two alloys were studied across the suite of testing—SAC 305 (Sn-3.0Ag-0.5Cu) and "Violet" (Sn-2.25Ag-0.5Cu-6.0Bi); compositions are given in wt.%. Firstly, a comprehensive aging study was undertaken to approximate the solvus of Bi in Violet; the outputs of this study helped to define an appropriate heat treatment temperature and duration. Next, the effects of the heat treatment on the following were studied:

- β-Sn grain structure,
- Creep resistance, and
- Accelerated thermal cycling (ATC) reliability.

The main objectives of this work are to quantify the benefits not only of including Bi in solder alloys, but also of *engineering* the alloy microstructure to yield further improvements in microstructure, properties, and reliability, ultimately prolonging the life of interconnects and electronic devices.

SOLVUS CHARACTERIZATION

Methodology

Bulk samples of Violet were prepared from larger ingots 50 g in size. These ingots were melted (alloy melting range is 205–210°C[7]) in clean graphite crucibles on a laboratory hot plate set at approximately 300°C and cut in half using a hacksaw with dedicated blade to avoid contamination; this process was repeated until four samples roughly 12 g in size were cast. This procedure was used to ensure compositional uniformity within all samples. Samples were cooled in air in standard ambient conditions.

Samples were then aged at one of four temperatures, i.e. 50°C, 70°C, 100°C, or 125°C, for 48 h in a box oven. These temperatures were selected based on the solvus temperature of the binary Sn-6Bi

alloy, which has the same Bi content as Violet. It is anticipated that the true solvus of Violet lies somewhere above that of Sn-6Bi due to the presence of Ag and Cu in the former—these species have limited solubility in the β-Sn matrix and will thus limit the amount of soluble Bi.

Samples were metallographically prepared using a series of progressively finer SiC grinding papers, followed by 3 μm diamond and colloidal silica polishing. Scanning electron microscopy (SEM) was used to examine the alloy microstructure using a Hitachi SU3500 instrument operated in backscattered electron (BSE) imaging mode, at 20 kV accelerating voltage. Images were acquired at 500× and 2500×; Bi precipitate size was quantified using 2500× images using thresholding in ImageJ software, and precipitate diameters (in μm) are reported. The original image resolution was approximately 20 pixels per micron; only particles greater than 5 pixels (0.25 μm) were included in the analysis, to minimize noise.

Results and Discussion

Some representative SEM images of Violet are shown in Fig. 1. The as-solidified alloy displays a dendritic microstructure typical of Sn-rich solders (Fig. 1a). No primary Ag_3Sn or Cu_6Sn_5 intermetallic compound (IMC) particles are observed, and it is evident that these are only present in the interdendritic region as secondary or ternary eutectics with β-Sn. In addition, Bi precipitates are visible in these regions. As the solid solubility of Bi in Sn decreases with temperature, it is likely that as the alloy solidifies and cools, Bi is rejected from the β-Sn matrix into the remaining melt, which constitutes the interdendritic region. The supersaturation of Bi in this region promotes precipitation of a secondary Bi phase. In addition, some Bi remains in solid solution within Sn dendrites; the solubility at room temperature is roughly 1.5 wt.%.[16]

For all aging temperatures, Bi precipitates appeared to migrate into the β-Sn dendritic regions, producing a more uniform distribution. The solubility of Bi in β-Sn increases with temperature, and thus the migration of Bi occurs via solid-state diffusion. Upon cooling, Bi will precipitate out of solid solution, and the microstructure will become more uniform as the aging temperature is increased.

Two distinct types of microstructures were observed. At the lower aging temperatures (50°C and 70°C), a more bimodal Bi precipitate size distribution was observed (Fig. 1b, c). Most precipitates were relatively small, on the order of microns, while several were very large, on the order of tens of microns. Higher-magnification imaging reveals the
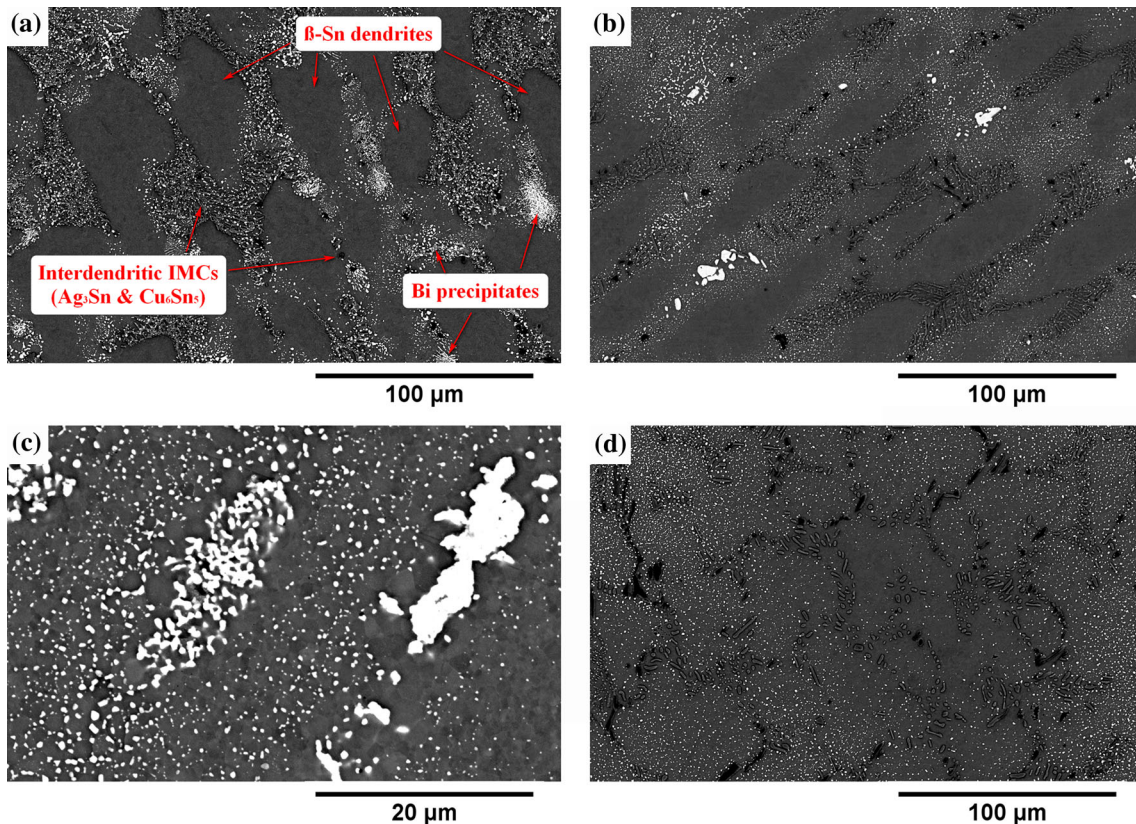

Fig. 1. Evolution of microstructure of Violet after isothermal aging: as solidified, 500×, with phases labeled (a); after aging at 70°C, 500× (b) and 2500× (c), after aging at 125°C, 500× (d).

presence of a precipitate-free, or denuded zone around these coarse Bi precipitates (Fig. 1c). These features suggest that a coarsening phenomenon such as Ostwald ripening occurred—during aging, some larger precipitates remained out of solid solution, and smaller precipitates dissolved into the β-Sn matrix. These dissolved Bi atoms, in addition to migrating into the β-Sn dendrites, may migrate towards the larger precipitates to reduce the interfacial phase boundary energy. At the higher aging temperatures (100°C and 125°C), no coarsened precipitates were observed, and precipitation occurred more uniformly, with respect to both distribution and precipitate size (Fig. 1d). At these temperatures, it is likely that all Bi entered solid solution and was able to diffuse throughout the β-Sn matrix.

Statistical analysis of the precipitate size is given in Table I. Aging the alloy at 50°C and 70°C results in a higher average precipitate size, as well as a wider size distribution; this is indicative of Ostwald ripening. Aging the alloy at 100°C and 125°C decreases the average precipitate size as well as the size distribution. These results suggest that the solvus temperature of Violet lies somewhere between 70°C and 100°C.

GRAIN STRUCTURE

Methodology

Ingot samples of both SAC 305 and Violet were prepared as described above. Two aging temperatures were selected, one above the approximate solvus and one below. The below-solvus temperature, 70°C, closely mimics in-service joint temperatures and was found in prior microstructural analysis to produce coarsened Bi precipitates. The above-solvus temperature, 125°C, was found to produce a highly uniform dispersion of Bi precipitates in the β-Sn matrix. Both alloys were aged at both temperatures for either 6 h, 24 h, 50 h, or 300 h. Alloys were also analyzed in the as-cast conditions.

Samples were metallographically prepared using a series of progressively finer SiC grinding papers, followed by 3 μm diamond and colloidal silica polishing. Further polishing was conducted using a Hitachi IM4000 ion mill. Each sample was polished for 5 min at a tilt of 7° at an accelerating voltage of 3 kV. This step removes any residual deformation introduced during metallography and ensures optimal signal collection from electron backscatter diffraction (EBSD) analysis.

Samples were characterized using an EBSD detector equipped on the same Hitachi SU-3500 VP-SEM used in the experimental solvus experiments. The SEM was operated at 20 kV in high-vacuum mode at a sample tilt of 70°. EBSD maps were collected using AZTEC software; further optimization of the maps was performed using HKL software. Grain size was calculated using HKL software and is reported as equivalent circle diameters in μm. In this analysis, all grains with a size of less than 20 pixels were excluded, and the low-angle grain boundary misorientation limit was defined as 15 degrees. Inverse pole figure (IPF) coloring, in the "z" direction, is used to display variations in sample texture.

Results and Discussion

Similar to precipitate distribution evolution, the grain structure of Violet underwent substantial changes during aging (Fig. 2). The initial grain structure is relatively coarse, with an interlaced β-Sn structure, which is commonly observed in SAC solder joints.[17] Over time, the alloy undergoes significant recrystallization; this is likely the result of a strain recovery. At 125°C, Bi can completely enter solid solution and diffuse through the β-Sn matrix. Upon cooling, Bi is forced out of solid solution and forms a second phase precipitate. Bi possesses a different crystal structure and density from Sn, such that there exists a structural mismatch between the two phases, which imposes strain on the softer β-Sn matrix. It is hypothesized that the resulting recrystallization is caused by particle stimulated nucleation (PSN), a phenomenon more commonly seen in highly stressed aluminum alloys.[18] As Sn is a very soft metal and highly active at room temperature due to its low melting point, even moderately low strain levels caused by Bi precipitation appear to be sufficient to trigger PSN. It is unknown whether recrystallization occurs prior to cooling. Further investigation is needed, using in situ EBSD.

The degree of recrystallization appears to peak after 50 h of aging. The extent of recrystallization is less after below-solvus aging at 70°C, compared with above-solvus aging at 125°C (Fig. 2f). This is

Table I. Precipitate diameter of violet samples

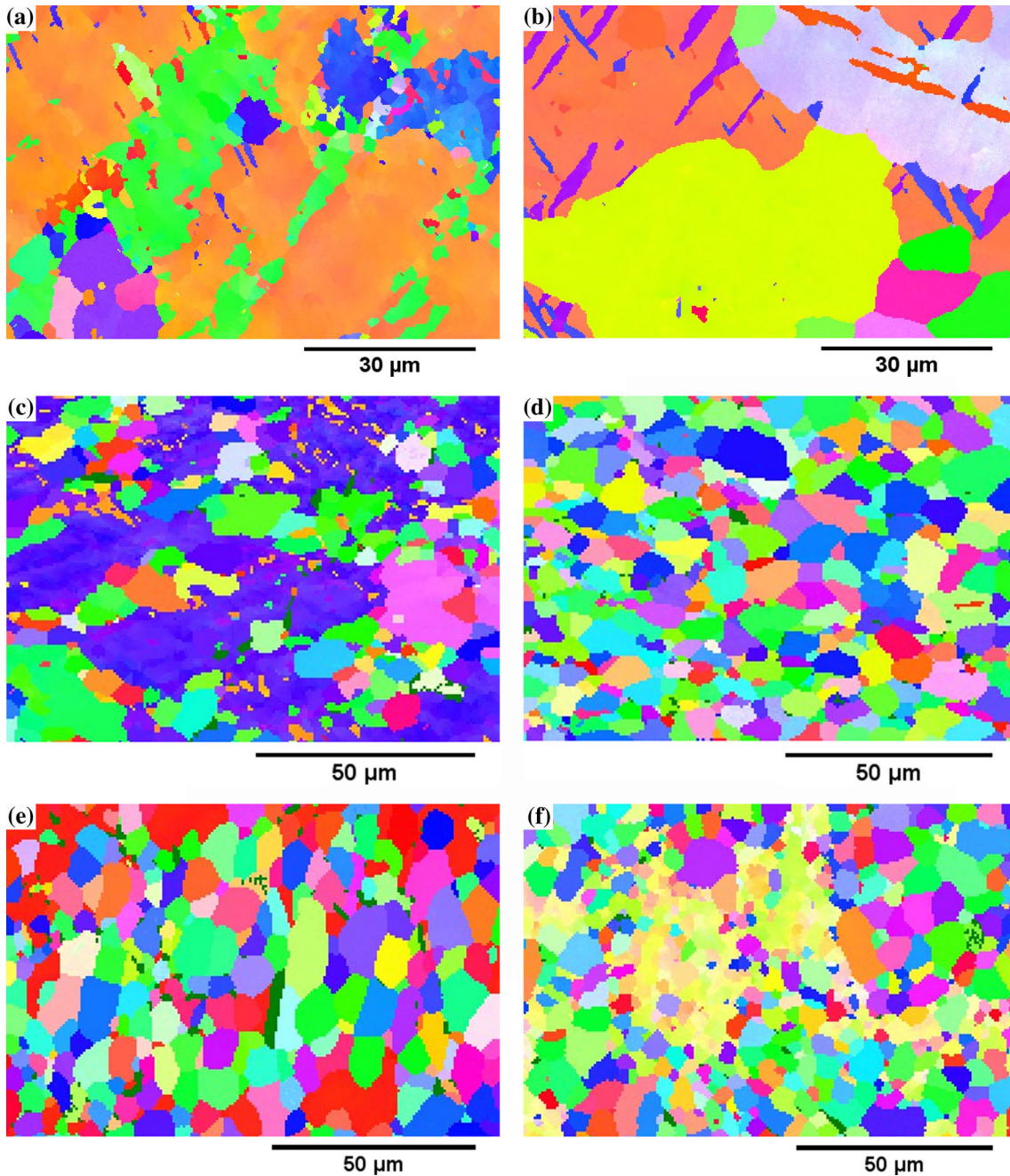| Aging temperature	Average precipitate diameter (μm)	Standard Deviation (μm)
As-cast	0.55	1.45
50°C	0.71	2.00
70°C	0.72	1.60
100°C	0.50	1.03
125°C	0.45	0.55

Fig. 2. Representative EBSD maps of Violet after aging (reprinted with permission of Ref. 33). As-solidified alloy (a); aged alloy at 125°C for 6 h (b), 24 h (c), 50 h (d), and 300 h (e); aged alloy at 70°C for 300 h (f).

likely due to the reduced mobility of Bi at lower temperature, as well as reduced solid solubility.

Grain size analysis indicated that the average grain size decreases as aging time increases, and the distribution of grain size becomes narrower (Fig. 3). In addition, the error bars are highly asymmetrical, with the upper limit of error greater than the lower limit. This feature is indicative of the transformation of large β-Sn grains into smaller, equiaxed grains as aging proceeds and Bi is allowed to distribute more uniformly. Statistically, there is

no significant difference between the two temperatures after 300 h of aging, the distribution is slightly wider after aging at 70°C.

In SAC 305, the grain size was significantly larger than that of Violet, and the structure did not change appreciably during aging, remaining coarse throughout (Fig. 4). For all EBSD maps shown in this work, only the orientation of β-Sn is given; secondary phases are displayed as "zero solutions," or were averaged out using post-processing in HKL.

CREEP ANALYSIS

Methodology

Similar-sized bulk samples of both SAC 305 and Violet were cast and metallographically prepared using a similar method as described above. These samples were subjected to one of five aging treatments, each consisting of combinations of below- and above-solvus aging. These treatments are summarized in Table II. In the treatments consisting of two steps, the second step was performed
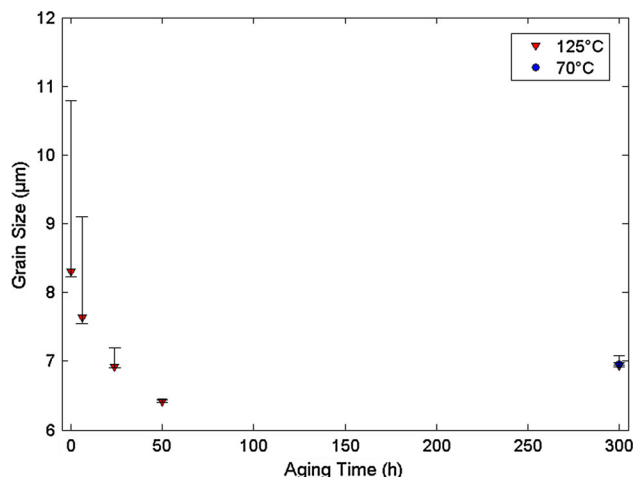

Fig. 3. Grain size of Violet after aging. The 300 h data points for 70°C and 125°C yielded similar results; the error bar is slightly wider for the former.

immediately after the first. It is noted that while the optimal grain structure was achieved after 50 h in the grain structure study above, the restorative treatments used in the creep study were shorter in duration. This is to more accurately reflect a more feasible scenario (reduction in thermal damage) if a restorative treatment were to be implemented in actual products.

RESULTS

Secondary creep rates were calculated using displacement/time data from 1500–3500 s. As creep testing was performed using nanoindentation, tertiary creep was not reached. It is also noted that rates reported in this work are not creep strain rates, which is typical of a tensile or compressive creep test, but rather displacement of the Berkovich tip over time. It has been shown in the literature that calculating creep strain rates using nanoindentation data is a challenging endeavor and was beyond the scope of this work.[19]

Secondary creep rates for each of the aging treatments are shown in Fig. 5. It is noted that there is no clear trend in the creep rate of SAC 305 with respect to the various heat treatments. This is an unexpected result, as SAC 305 tends to undergo degradation of mechanical properties after aging.[1,2] In this case, nanoindentation is a local measurement, and thus may not necessarily be indicative of bulk mechanical properties. In addition, secondary phases such as IMCs may be present below the surface and can influence the material's response to
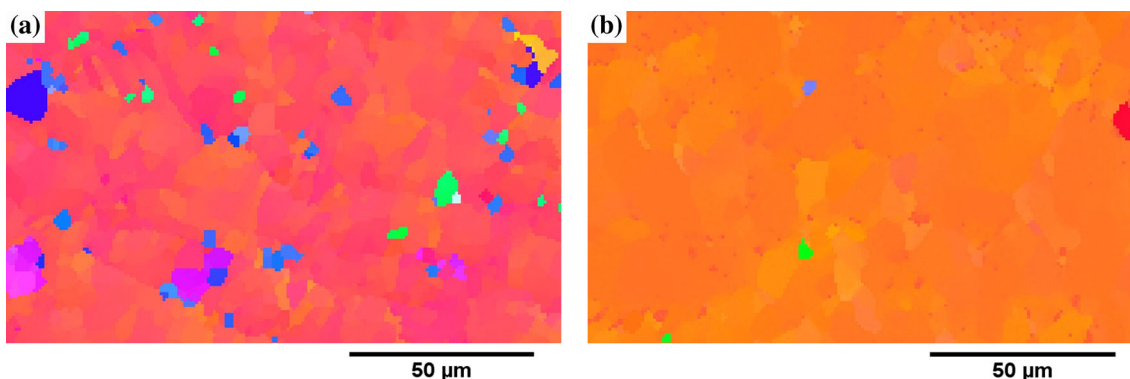

Fig. 4. Representative EBSD maps of SAC 305 after aging (reprinted with permission of Ref. 33). As-solidified alloy (a); aged alloy at 125°C for 24 h (b). The smaller grains of different orientation are artifacts from the sample preparation process.

Table II. Creep analysis aging treatments

Representative conditions	Step 1	Step 2
Post-reflow	As-cast	N/A
Extended field service	70°C, 300 h	N/A
Short restoration treatment following extended field service	70°C, 300 h	125°C, 12 h
Longer restoration treatment following extended field service	70°C, 300 h	125°C, 24 h
Ideal microstructural conditions after thermal treatment	125°C, 300 h	N/A

122

Delhaise, P. Snugovsky, Kennedy, Hillman, Matijevic, Meschter, Adams, Kammer, Romansky, Juarez, Straznicky, L. Snugovsky, Wilcoxon, and Perovic
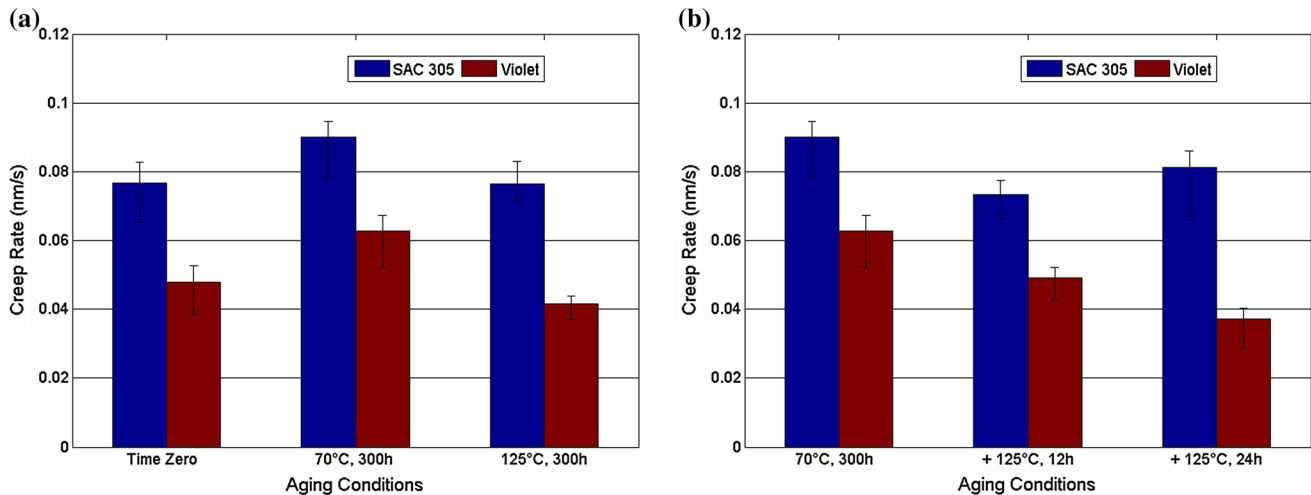
Fig. 5. Secondary nanoindentation creep rates of SAC 305 and Violet with respect to heat treatment(s). Comparison of as-cast alloy to aged alloy for 300 h at 70°C and 125°C (a); effect of restoration treatments on alloy aged at 70°C for 300 h (b).

indentation. For Violet, it is observed that aging the alloy at 70°C increases the secondary creep rate, while aging at 125°C decreases the creep rate (Fig. 5a). Figure 5b shows the effects of short restorative heat treatments on the creep rate of the alloy aged at 70°C for 300 h (representing extended time in service). It is observed that the restorative treatments at 125°C dramatically improve the creep properties of Violet. For example, restoring the alloy for 24 h decreases the creep rate by over 35%. Furthermore, the 125°C, 24 h restoration treatment yields comparable creep rates as the extended aging treatment for 300 h, indicating that it may not be necessary to use extended aging treatments to improve alloy properties.

Suggested Mechanisms

The mechanism of creep deformation is strongly material-dependent; however, it has been suggested that owing to their low melting points, solder alloys likely deform via a diffusion mechanism.[20] Coble creep consists of diffusion of vacancies along short-circuit pathways such as high-angle grain boundaries,[21] which tend to facilitate greater mass transport than through the lattice. This is manifested by grain boundary sliding. Based on this model, it is anticipated that a highly polycrystalline material with significant grain boundary content will be less resistant to diffusional creep. In addition, deformation may be influenced by second phase precipitates. These act to impede dislocation motion—depending on size, one of two interactions are possible—Friedel cutting or Orowan bowing.[21] Zener pinning occurs when the movement of grain boundaries is retarded by second phase precipitates,[22] and this effect may influence Coble creep in polycrystalline materials.

In this study, the creep resistance of the as-cast Violet alloy was superior to that of SAC 305, likely due to the increased second phase precipitate content. After above-solvus aging, Bi was able to diffuse more uniformly throughout β-Sn and, via PSN,[18] was able to produce a highly polycrystalline recrystallized grain structure. While this increase in grain boundary content should make Coble creep more favorable than in the as-cast alloy, the homogenous dispersion of Bi precipitates, many located at grain boundaries, appear to have exerted a counteractive Zener pinning mechanism which limited vacancy diffusion along grain boundaries and therefore sliding. The relative lack of sensitivity of the creep resistance to below-solvus aging may be explained by a lesser extent of recrystallization and Zener pinning due to the less uniform Bi dispersion. In addition, dislocations may bow around Ostwald ripened precipitates; theoretically, this action would require lower applied stress.[15]

Similar results have been observed in other studies of creep in Bi-containing solder alloys. Vianco[20] found that isothermal aging of Sn-3.4Ag-4.8Bi improved creep properties by "adding obstacles" to deformation (likely a uniform dispersion of Bi precipitates and Zener pinning) as well as a more active diffusion mechanism for creep (likely increased grain boundary content).

ACCELERATED THERMAL CYCLING

Test Vehicle

The printed circuit board (PCB) was 0.081 ± 0.008 inches thick and constructed using FR-4 and eight dummy inner layers, per the IPC-4101 specification. PCBs were finished using immersion silver (ImmAg). The package studied was a Land Grid Array (LGA) component to avoid mixed metallurgy conditions and ensure the Violet paste was not diluted into a SAC 305 solder ball. The packages were 17 mm × 17 mm, 256 I/O (Practical Components part number A-CABGA256-1.0 mm–17 mm-DC). Sixty components were placed on each test vehicle, and the parts were daisy-

chained to allow for resistivity monitoring throughout the thermal cycling test (Fig. 6).

Assembly and Preconditioning

Twelve test vehicles in total were assembled—six using SAC 305 paste and six with Violet paste. The solder pastes were applied using an MPM Ultraprint 2000 stencil printer with 0.005 inch stainless steel stencil. Using a Universal GC-120 machine, the components were then placed on the test vehicles. The test vehicles with both alloys were reflowed in a Heller 1912EXL Convection Reflow Oven. The oven was operated at a conveyor speed of approximately 1.1 m/min and a nitrogen flow rate of approximately 42.5 m^3/h.

After cooling, the assembled test vehicles were placed in an Electrovert Aquastorm 200 inline cleaning system for removal of contaminants and solder flux residues. The cleaning agent used was Kyzen Aquanox A4625 saponifier in deionized water. The final step prior to accelerated thermal cycling was to precondition the solder joints on several of the assemblies. Of the three test vehicles per alloy per thermal cycle, one was left in as-assembled conditions, and the other two were subjected to preconditioning treatments at 125°C—one for 24 h and the other for 48 h.

Reliability Testing

Two thermal cycles were selected: −55°C to 125°C and −40°C to 70°C. Testing was conducted in accordance with the IPC-9701 specification, using 15 min temperature dwells at each temperature extreme, along with a temperature ramp of 5–10°C/min. The −55°C to 125°C cycle is a standard thermal cycling range in the IPC specification and is commonly used in product qualifications in the aerospace and defence industry. In this cycle, it is expected that Bi dissolution / precipitation will be

Fig. 6. Populated test vehicle for ATC testing (reprinted with permission of Ref. 34).

highly dynamic. The −40°C to 70°C is not a standard range in the specification; however, all requirements were met. The upper dwell temperature of 70°C was deliberately selected to be lower than the predicted solvus temperature of Violet, and thus it is believed that during the entire duration of the test, some Bi should remain out of solid solution.

Through-holes were routed along one side of the test vehicle for ease of organizing cabling to the test vehicle. Instead of using a connector to electrically connect the daisy-chain circuits to the continuity monitoring equipment, ribbon cable leads were manually soldered to the through-holes corresponding to each component I/O pair. An Anatech event detection system was used to monitor the continuity of the daisy-chained components over the course of the thermal cycling testing. Each component was individually monitored, and an "event" was recorded if, within a 30 s time frame, the resistance of the channel exceeded 300 O for longer than 0.2 μs. A failure was defined when one of the following criteria was met:

- The 300 O resistance was exceeded for 15 consecutive events,
- Five consecutive detection events were detected, followed by at least 15 nonconsecutive events, or
- An electrical open was detected.

The Anatech system chronologically records the cycle number and chamber temperature at the time of all individual events—once the system has deemed the component to have failed based on any of the above criteria, no further event data are recorded from that component for the remainder of the test.

RESULTS

The failure distributions were fitted to the two-parameter Weibull function and reliability plots for each test as shown in Fig. 7. A summary of the reliability data is shown in Table III. In both Fig. 7 and Table III, "ASM" indicates "as manufactured." In Fig. 7, the times "24 h" and "48 h" indicate the heat treatment of 125°C for either 24 or 48 h.

Figure 7a shows that the heat treatment had a negligible effect on the reliability after the harsher cycle between −55°C and 125°C for both alloys, and that the reliability of components assembled using Violet was approximately two times larger than those assembled using SAC 305. SAC 305 demonstrated more variation between the heat treatment conditions and there was no impact of the heat treatment on the reliability of Violet. Under the milder ATC conditions between −40°C and 70°C (Fig. 7b), SAC 305 outperformed Violet and yielded fewer overall failures (including zero from the cell heat treated for 24 h). It is noted that the reported Weibull parameters reported for SAC 305 for this cycle are not statistically accurate due to the low
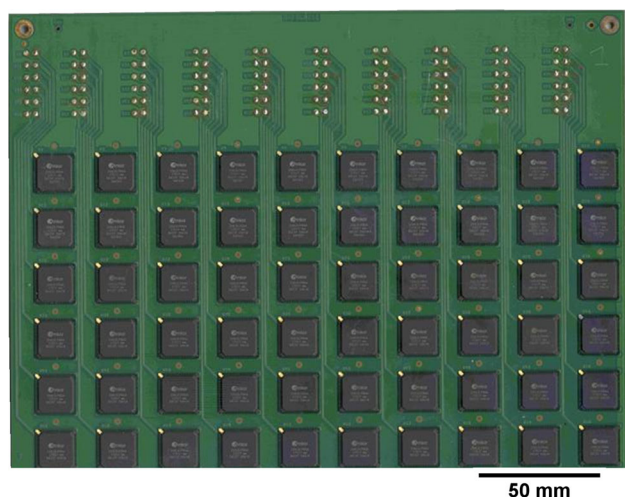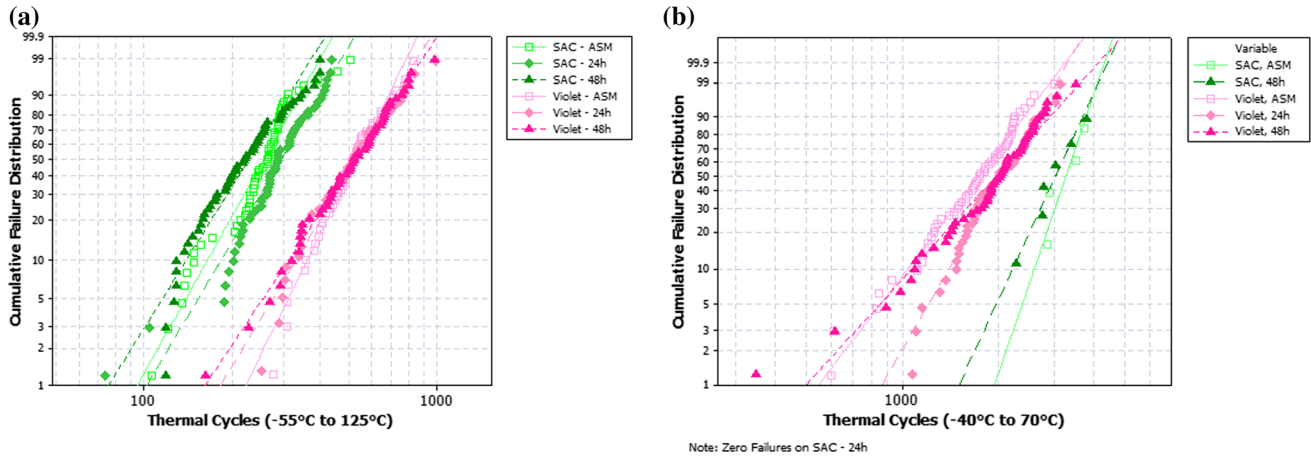
Fig. 7. Weibull reliability plots for −55°C to 125°C cycling (a) and −40°C to 70°C cycling (b).

Table III. Summary of ATC reliability data

ATC range	Heat treatment	Alloy	Failure rate (%)	θ	β	μ
−40°C to 70°C	ASM	SAC 305	8	3421	8.26	0.910
		Violet	98	1923	3.68	0.993
	125°C, 24 h	SAC 305	0	N/A	N/A	N/A
		Violet	98	2231	4.87	0.987
	125°C, 48 h	SAC 305	10	3221	6.10	0.981
		Violet	98	2221	3.10	0.980
−55°C to 125°C	ASM	SAC 305	100	281	4.26	0.969
		Violet	98	579	4.85	0.985
	125°C, 24 h	SAC 305	97	324	4.00	0.969
		Violet	98	587	3.97	0.980
	125°C, 48 h	SAC 305	100	252	3.84	0.967
		Violet	98	589	3.58	0.996

failure rates.[23] The heat treatment did provide some improvement to the reliability of Violet, increasing the characteristic lifetime by around 300 thermal cycles. The data from the Violet joints treated for 24 h is nearly identical to that from joints treated for 48 h.

In Table III, the "failure rate" indicates the number of samples, out of a population of 60 samples for each combination that had failed by the end of testing. The values of the Weibull coefficients, θ and β, were determined using Minitab software regression fitting. The results in Table III also exclude failures within the first 40 thermal cycles, which are deemed to be the result of infant mortality. Most test combinations showed no more than one of these early failures out of the initial population of 60 components.

All samples demonstrated similar failure modes through the bulk solder (Fig. 8).

Suggested Mechanisms

It has been widely agreed that deformation in Pb-free solder joints in accelerated thermal cycling occurs via a series of metallurgical changes. In the region of highest stress concentration (often on the side of the joint closest to the package or at solder mask-defined pads [24]), coarsening of second phase particles (e.g. Ag_3Sn) occurs first,[25] followed by rotation of Sn grains to relieve the building defect density (recovery). Then, recrystallization occurs, involving the consumption of highly strained defect-rich grains by a new low-strain, highly equiaxed β-Sn grain structure.[26] Finally, crack propagation proceeds through the high-angle grain boundary network among the recrystallized region.

In metals and alloys, the effectiveness of recovery during deformation is dictated by the stacking fault energy (SFE). The SFE determines the degree of dissociation of a dislocation into two partial dislocations and thus the width of the imperfect crystalline region bounded by the partials, known as a stacking fault. The width of the stacking fault dictates the propensity of dislocations to undergo climb and/or cross slip, which are well-known mechanisms of recovery.[27] With a higher SFE, stacking faults are narrower, recovery is more effective, and recrystallization will initiate later.[28] Dislocations in a material with a lower SFE will dissociate more easily, producing wider stacking
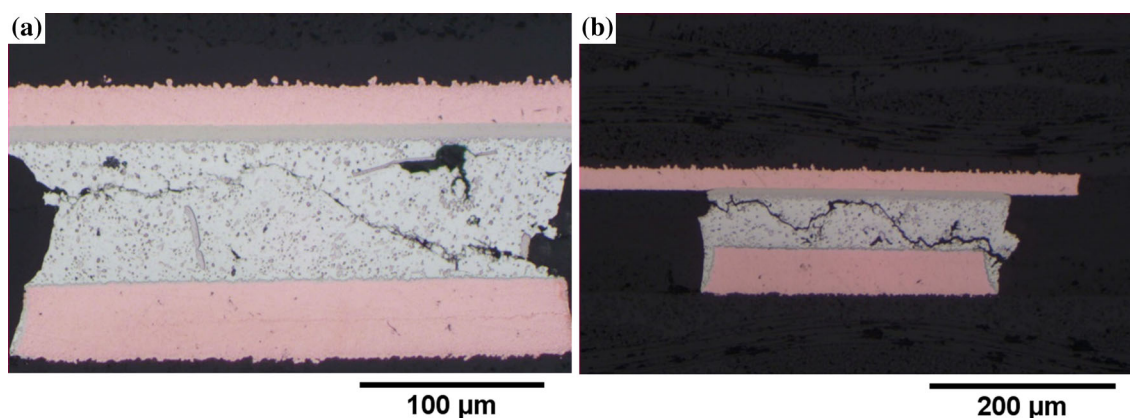
Fig. 8. Example optical micrographs of failed LGA samples after −40°C to 70°C cycling (reprinted with permission of Ref. 34). SAC 305, preconditioned for 48 h (a); Violet, preconditioned for 48 h (b).

faults and making climb and cross slip difficult.[27] This results in recrystallization initiating sooner.

The magnitude of cyclic strain can also dictate whether recovery or recrystallization dominates. Initially, recovery releases some of the accumulated strain energy via dislocation climb and/or cross slip. However, the accumulation rate is greater than the release rate, resulting in a net accumulation of plastic strain in the joint during cyclic deformation.[26] At some critical level of strain (dislocation density), recovery will cease to be effective, and recrystallization will initiate.[28] In harsher thermal cycles (with greater ΔT) more plastic strain is accumulated with each cycle. Thus, recovery is less effective, and recrystallization initiates sooner. Milder cycles generally yield less plastic strain accumulation per cycle, and recovery occurs for longer durations.[26]

Furthermore, it has been observed in other alloy systems that alloying reduces SFE. For example, the SFE of pure Cu is roughly 58 mJ/m^2, and that for an alloy with 15 at.% of aluminum is roughly 5 mJ/m^2.[29] While SFE data for Sn-Bi is currently unknown, it has been determined that pure Sn has a very high SFE,[28] with a recent study, using density functional theory, reporting a value of approximately 200 mJ/m^2 in its easiest slip system.[30] This would suggest that pure Sn undergoes substantial recovery prior to recrystallization, and that Sn-based alloys will undergo recrystallization sooner owing to reduced SFE. It is likely that Bi has a stronger effect on suppressing SFE than Ag or Cu due to its greater solid solubility in β-Sn.

It is believed that during the harsher −55°C to 125°C cycling, Bi will enter solid solution and diffuse throughout the β-Sn matrix, very much like during isothermal aging. Very little is understood about the kinetics of dissolution and precipitation of Bi into/out of solution during heating and cooling, respectively, due to combined thermal and strain enhanced diffusion. Examination of the literature has revealed that dissolution of Bi at elevated temperatures occurs on the order of minutes.[31]

Precipitation, on the other hand, may occur substantially slower.[32] Based on these results, it can be suggested that dissolution of Bi occurs faster during the ramp up/hot dwell than does precipitation during the ramp down/cold dwell. If so, Bi would gradually accumulate in solid solution with β-Sn and remain largely in this state during the test.

In −55°C to 125°C cycling, recrystallization is more dominant due to the greater net plastic strain accumulation per cycle. Even though Violet should be more susceptible to recrystallization assuming a lower SFE, it demonstrated improved reliability over SAC. This result may be the cause of competing mechanisms—Bi, whether in solid solution or as a second phase precipitate, will strengthen the alloy. As the hot dwell temperature is substantially higher than solvus, Bi is easily able to enter solid solution and diffuse throughout the β-Sn matrix. This may explain the lack of effect of preconditioning on the ATC performance of Violet in these cycling conditions.

In the milder −40°C to 70°C cycling, the net accumulation of plastic strain in the joint is substantially slower owing to the lower ΔT and thus recovery will dominate. As SAC 305 likely has a higher SFE than Violet, recrystallization in Violet would commence sooner, resulting in lower reliability given the same thermal cycling parameters. Because the hot dwell in this cycle (70°C) appears to lie below the predicted solvus temperature of Violet, it is likely that some amount of Bi will remain out of solution for the entire duration of the test and Ostwald ripening will take place. The Bi in the preconditioned alloy will initially be more homogeneously distributed, which suggests that less Ostwald ripening would occur. Assuming coarsened Bi precipitates are a detriment to reliability, this would explain the slight improvement in ATC performance of preconditioned Violet joints over as-assembled joints.

Finally, it is stressed that this ATC experiment was conducted using a single CABGA package and PCB (laminate, layup, and surface finish), and

changing any one of these parameters may influence the results. It is, therefore, highly recommended to perform similar experiments with different modifications to the test vehicle to verify if these trends hold.

FUTURE WORK

It is of interest to examine the effects of preconditioning and/or restoration on the grain structure of solder joint-sized samples. While the cooling rates of the bulk samples in this study were comparable to those commonly observed in reflow, it is important to verify whether the same trends occur in solder joints.

There are ongoing efforts to evaluate both the time-independent (stress-strain) and time-dependent (creep) properties of the Violet alloy, both before and after aging, using compression testing and a similar approach to that by Vianco.[20] Microstructure will be examined before and after testing to study the effects of Bi and aging on the deformation characteristics of the alloy. In addition, the outputs from this testing will be used to create a thermomechanical model of the Violet alloy, which will allow the alloy to be registered by governmental agencies. This is a necessary step towards the commercialization of the alloy.

In this study, we demonstrated that subjecting the alloy to restorative treatments after simulated service time (below-solvus aging) improved the creep resistance. The next logical step would be to test the effects of injecting restoration treatments into a board level reliability test. Future work is planned in which a reliability test (thermal cycling and/or vibration) will be conducted, with some assemblies being tested uninterrupted, while others are subjected to periodic heat treatments before being returned to the testing chamber. The goal of this test is to evaluate whether service life can be extended via restoration.

Previous work has shown that dissolution of Bi into β-Sn upon isothermal heating appears to occur faster than precipitation of Bi out of solid solution upon cooling.[31,32] It is planned to extend the previous in situ dissolution study by quantifying the effects of initial precipitate spacing, consideration of multiple dissolution temperatures, and utilizing forced cooling to study precipitation. In situ EBSD could also be used to directly observe PSN. It may be possible to mimic reliability testing and examine the mobility of Bi during an in situ thermal cycling test.

It was surmised that recovery is less effective in Violet during ATC due to reduced stacking fault energy, which affects performance in thermal cycling reliability. It is possible to use transmission electron microscopy (TEM) to evaluate the SFE for Sn, Sn-Bi and SAC-Bi alloys to verify this hypothesis. Such a study would allow for a more in-depth understanding of how Bi influences the microstructure and properties of Sn-rich alloys at the atomic scale.

SUMMARY AND CONCLUSIONS

In this series of studies, we evaluated the effects of implementing a short, above-solvus heat treatment as a preconditioning or restoration process to improve the microstructure, properties, and reliability of third-generation Bi-containing Pb-free solder alloys. Preconditioning could be implemented immediately after reflow in tandem with processes such as underfill/edge bond curing, which is often conducted at similar temperatures. Restorative treatments could be performed during periodic preventive maintenance actions—unlike conventional repair processes, there would be no need to remove and replace components. As a result, the overall expenses incurred during the product life cycle would be reduced, as fewer replacement parts are consumed, the PCB experiences less damage, and less time is spent troubleshooting possible solder joint failures.

The results from this work can be summarized as follows:

- Using a series of aging experiments, the solvus of Violet was estimated to be between 70°C and 100°C. After aging at 70°C and below, Ostwald ripening of Bi precipitates appeared to occur, suggesting not all Bi entered the solid solution. After aging at 100°C and above, Bi precipitated uniformly, both in size and distribution, suggesting all Bi was able to dissolve in β-Sn.
- Based on the results from the solvus characterization study, a heat treatment temperature of 125°C was selected. The length of the heat treatment was chosen to be between 12 h and 48 h, though a 24 h duration may be more ideal to find a balance between limiting thermal damage and maximizing redistribution of Bi.
- The grain structure of Violet was shown to undergo recrystallization after aging. It is surmised that the recrystallization is caused by particle stimulated nucleation (PSN) when Bi emerges from solid solution, and mismatch (crystal structure) is created between the newly formed Bi precipitates and the β-Sn matrix.
- While no clear trends are evident comparing the creep resistance of SAC 305 with respect to any of the heat treatments, it was found that after simulated service life (below-solvus aging), the creep resistance of Violet is increased slightly. The creep resistance undergoes marked improvements after subsequent above-solvus aging, suggesting that the properties of Violet not only can be restored, but can be improved after heat treatment.
- SAC 305 and Violet behaved very differently with respect to one another at each of the two cycles. For the harsher −55°C to 125°C cycling, Violet outperformed SAC likely due to solid solution strengthening from the Bi constituent. However, the opposite trend was observed after

the milder −40°C to 70°C cycling. It is suggested that this variance may be the result of differences in the susceptibility of each alloy to undergoing recovery and recrystallization during deformation, as well as the propensity of each cycle to induce these microstructural changes.

- Preconditioning appeared to have no significant effect on the ATC reliability of either SAC 305 or Violet after −55°C to 125°C cycling. After −40°C to 70°C cycling, however, the characteristic life of Violet was improved by roughly 15%. This is believed to be the result of a more initially homogeneous distribution of Bi in the alloy prior to cycling, which would delay the onset of Ostwald ripening.
- This work demonstrates the combined potential of Bi-containing alloys and preconditioning/ restoration in improving the properties and reliability of solder joints. Although the ATC test was performed with just a single part type and testing with alternative parts is recommended, it is evident that a number of factors need to be considered when selecting a Pb-free alloy for a specific application.

REFERENCES

1. H. Ma, J. Suhling, Y. Zhang, P. Lall, and M.J. Bozack, in *Electronic Components and Technology Conference Proceedings* (2007), pp. 653–658.
2. M. Hasnine, M. Mustafa, J.C. Suhling, B.C. Prorok, M.J. Bozack, and P. Lall, in *2013 Electronic Components and Technology Conference Proceedings* (2013), pp. 168–178.
3. R. Coyle, J. Smetana, D. Hillman, C. Johnson, R. Parker, B. Sandy-Smith, H. Zhang, J. Geng, M. Osterman, B. Arfaei, A. Delhaise, K. Howell, J. Bath, S. Longgood, A. Kleyner, J. Silk, R. Pandher, E. Lundeen, and J. Noiray, in *SMTA International Conference Proceedings* (2018).
4. P.T. Vianco and J.A. Rejent, *J. Electron. Mater.* 28, 10 (1999).
5. Z. Moser, W. Gasior, K. Bukat, J. Pstrus, R. Kisiel, J. Sitek, K. Ishida, and I. Ohnuma, *J. Phase Equilib. Diffus.* 27, 2 (2006).
6. D. Witkin, in *APEX Expo Proceedings* (2013), pp. 540–560.
7. J. Juarez, P. Snugovsky, E. Kosiba, Z. Bagheri, S. Subramaniam, M. Robinson, J. Heebink, J. Kennedy, and M. Romansky, *J. Microelectron. Electron. Packag.* 12, 1 (2015).
8. N. Jadhav, M. Williams, F. Pei, G. Stafford, and E. Chason, *J. Electron. Mater.* 42, 2 (2013).
9. D. Witkin, *J. Electron. Mater.* 41, 2 (2012).
10. A. Delhaise, L. Snugovsky, D. Perovic, P. Snugovsky, and E. Kosiba, *J. Surf. Mt. Technol.* 27, 3 (2014).
11. A. Delhaise, D. Perovic, and P. Snugovsky, *J. Surf. Mt. Technol.* 30, 2 (2017).
12. T.-K. Lee, T. Bieler, C.-U. Kim, and H. Ma, *Fundamentals of Lead-Free Interconnect Technology*, 1st ed. (New York: Springer, 2015), p. 81.
13. A. Delhaise, Z. Chen, and D. Perovic, *J. Electron. Mater.* 47, 3 (2018).
14. A. Delhaise, Z. Chen, and D. Perovic, *JOM* 71, 1 (2019).
15. E. Arzt, *Acta Mater.* 46, 16 (1998).
16. B.-J. Lee, C.-S. Oh, and J.-H. Shim, *J. Electron. Mater.* 25, 6 (1996).
17. T.-K. Lee, T. Bieler, C.-U. Kim, and H. Ma, *Fundamentals of Lead-Free Interconnect Technology*, 1st ed. (New York: Springer, 2015), p. 93.
18. F.J. Humphreys and M. Hatherly, *Recrystallization and Related Annealing Phenomena*, 2nd ed. (Oxford: Elsevier, 2004), pp. 293–303.
19. J. Dean, A. Bradbury, G. Aldrich-Smith, and T.W. Clyne, *Mech. Mater.* 65, 1 (2013). https://doi.org/10.1016/j.mechmat.2013.05.014.
20. P. Vianco, J. Rejent, M. Grazier, and A. Kilgo, *Materials* 5, 11 (2012).
21. M.E. Kassner, *Fundamentals of Creep in Metals and Alloys*, 3rd ed. (Waltham: Butterworth-Heinemann, 2015), p. 91.
22. R.D. Doherty, D.A. Hughes, F.J. Humphreys, J.J. Jonas, D. Juul Jensen, M.E. Kassner, W.E. King, T.R. McNelley, H.J. McQueen, and A.D. Rollett, *Mater. Sci. Eng. A* 238, 2 (1997).
23. R.B. Abernathy, *The New Weibull Handbook*, 2nd ed. (North Palm Beach: Robert B. Abernathy, 1996), p. 31.
24. L. Yin, L. Wentlent, L. Yang, B. Arfaei, A. Oasaimeh, and P. Borgesen, *J. Electron. Mater.* 41, 2 (2012).
25. P. Boregsen, L. Wentlent, S. Hamasha, S. Khasawneh, S. Shirazi, D. Schmitz, T. Alghoul, C. Greene, and L. Yin, *J. Electron. Mater.* 47, 5 (2018).
26. J. Hokka, T. Mattila, H. Xu, and M. Paulasto-Kröckel, *J. Electron. Mater.* 42, 6 (2013).
27. F.J. Humphreys and M. Hatherly, *Recrystallization and Related Annealing Phenomena*, 2nd ed. (Oxford: Elsevier, 2004), p. 18.
28. T.T. Mattila and J.K. Kivilahti, *Recrystallization*, ed. K. Sztwiertnia (London: IntechOpen, 2012), p. 189.
29. Q. Shao, L. Liu, T. Fan, D. Yuan, and J. Chen, *J. Alloys Compd.* (2017). https://doi.org/10.1016/j.jallcom.2017.07.332.
30. M. Bhatia, I. Adlakha, G. Lu, and K. Solanki, *Scr. Mater.* (2016). https://doi.org/10.1016/j.scriptamat.2016.05.038.
31. P. Banh, A. Delhaise, and D. Perovic, *J. Surf. Mt. Technol.* 32, 2 (2019).
32. S. Belyakov, J. Xian, G. Zeng, K. Sweatman, T. Nishimura, T. Akaiwa, and C. Gourlay, *J. Mater. Sci. Electron.* 30, 1 (2019).
33. A. Delhaise, P. Snugovsky, I. Matijevic, J. Kennedy, M. Romansky, D. Hillman, D. Adams, S. Meschter, J. Juarez, M. Kammer, I. Straznicky, L. Snugovsky, and D. Perovic, *J. Surf. Mt. Technol.* 31, 1 (2018).
34. A. Delhaise, D. Hillman, P. Snugovsky, J. Kennedy, R. Wilcoxon, D. Adams, S. Meschter, J. Juarez, M. Kammer, I. Straznicky, and D. Perovic, *J. Surf. Mt. Technol.* 32, 1 (2019).